ACS APPLIED MATERIALS & INTERFACES

Research Article

www.acsami.org

In Vitro and in Vivo Studies on the Transport of PEGylated Silica Nanoparticles across the Blood–Brain Barrier

Dan Liu,[†] Bingqian Lin,[†] Wei Shao,[†] Zhi Zhu, Tianhai Ji,* and Chaoyong Yang*

Affiliated Chenggong Hospital, State Key Laboratory of Physical Chemistry of Solid Surfaces, the Key Laboratory for Chemical Biology of Fujian Province, The MOE Key Laboratory of Spectrochemical Analysis & Instrumentation, Department of Chemical Biology, College of Chemistry and Chemical Engineering, Xiamen University, Xiamen 361005, People's Republic of China

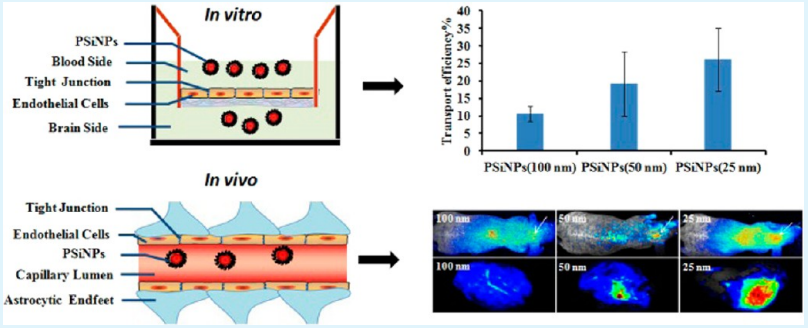

ABSTRACT: Transport of PEGylated silica nanoparticles (PSiNPs) with diameters of 100, 50, and 25 nm across the blood–brain barrier (BBB) was evaluated using an in vitro BBB model based on mouse cerebral endothelial cells (bEnd.3) cultured on transwell inserts within a chamber. In vivo animal experiments were further performed by noninvasive in vivo imaging and ex vivo optical imaging after injection via carotid artery. Confocal fluorescence studies were carried out to evaluate the uptake of PSiNPs by brain endothelial cells. The results showed that PSiNPs can traverse the BBB in vitro and in vivo. The transport efficiency of PSiNPs across BBB was found to be size-dependent, with increased particle size resulting in decreased efficiency. This work points to the potential application of small sized silica nanoparticles in brain imaging or drug delivery.

KEYWORDS: *PEGylated silica nanoparticles, blood–brain barrier, different size, transportation*

INTRODUCTION

The blood–brain barrier (BBB) formed by brain capillary endothelial cells is an important physiological barrier in the central nervous system that regulates the passage of molecules from the circulatory system into the brain. This barrier protects the brain from the invasion of various noxious agents. However, it also hinders the delivery of diagnostic and therapeutic agents to the brain.[1,2] Although various strategies have been proposed to overcome this barrier, including biochemical modification, osmotic opening of the cerebral capillary endothelium, as well as alternative routes for administration, they are largely limited by the chemical structures of the agents and the existence of efflux pumps.[3−5] Therefore, delivery of diagnostic and therapeutic agents across the BBB is still a major challenge for neurological disorders.

With the advent of nanobiotechnology, nanoparticles (NPs) with high chemical and biological stability functionalized by protective ligands are increasingly demonstrating superior over other strategies in BBB transport.[6−12] Nanoparticles with sizes between 1 and 100 nm serve as nanocarriers to enhance the delivery of agents across the BBB for imaging and therapy.[13] The underlying mechanisms of how NPs cross the BBB may include receptor or absorptive mediated transcytosis by endothelial cells,[14−16] opening of the tight junctions and inhibition of the transmembrane efflux systems, as well as other unknown mechanisms.[17−21] Transport of NPs across the BBB may depend on various factors, such as the surrounding surfactants, NP size, and electric charge.[22]

Currently, several types of NPs have been reported for enhancing the passage of agents across the BBB. For example, a study of the transport efficiency of lipid-based NPs carrying a calcium channel blocker drug showed that the drug was taken up to a greater extent by the brain and maintained high drug levels for a longer time than free drug suspension.[23] Also, Hasadsri et al. reported that polybutylcyanoacrylate (PBCA) NPs could be successfully utilized for delivery of functional proteins into neurons and neuronal cell lines.[24]

Compared with the above nanocarriers, silica nanoparticles (SiNPs) are of great interest because of their biocompatibility and extraordinary properties, such as relatively low cost, straightforward synthesis, facile surface modification, and partial urinary excretion.[25−30] Due to their unique characteristics, SiNPs have been widely used in a wide range of areas including biomedical and biotechnological applications.[31,32] To our knowledge, the transport of SiNPs across the BBB has not previously been investigated. Of special interest is the effect of

Received: November 20, 2013
Accepted: January 13, 2014
Published: January 13, 2014

Scheme 1. Schematic of PSiNP Transport across the BBB In Vitro (A) and *in vivo* (B)

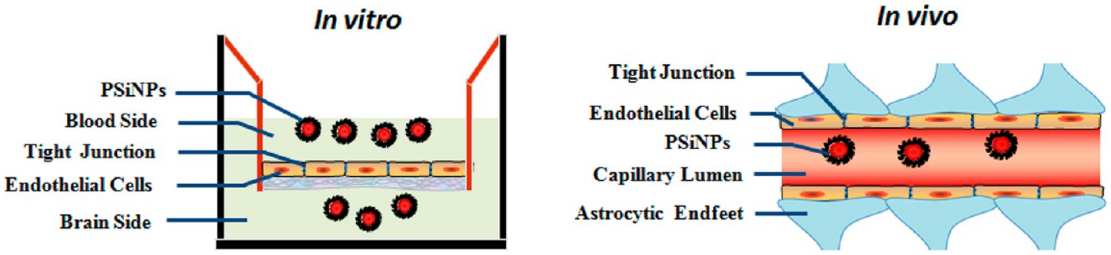

particle size, which can determine the distribution in vivo and biological fate of NP systems.[33] Many researchers have demonstrated that NPs of sub-micrometer size can provide a significant advantage over microparticles for drug delivery,[34,35] but the effect of particle size on BBB transport efficiency has not been sufficiently investigated. Previous research has shown that SiNPs modified with polyethylene glycol (PEG) can enhance the plasma residence time and reduce clearance by the reticulo-endothelial system (RES) system.[29] PEG may also increase the endothelial permeability of NPs and thus facilitate their BBB passage.[36]

In the present study, the transport of PEGylated SiNPs (PSiNPs) of three different sizes across the BBB was evaluated in vitro and in vivo, as shown in Scheme 1. To determine whether PSiNPs can traverse the BBB and how the particle size influences the efficiency, Rubpy dye was entrapped in PSiNPs as a fluorescent signal indicator to track the particles. The BBB transport efficiency was evaluated using an in vitro BBB model based on mouse cerebral endothelial cells (bEnd.3) cultured on transwell inserts within a chamber. In vivo animal experiments were performed by noninvasive in vivo imaging and ex vivo optical imaging after injection via carotid artery. Confocal fluorescence studies showed that the BBB transport efficiency of PSiNPs is inversely dependent on the size both in vitro and in vivo.

MATERIALS AND METHODS

Materials. Amino polyethylene glycol monomethyl ether (mPEG-NH_2, M_n = 2000) was purchased from Jiaxing Bomei Biological Technology Co., Ltd. Lactoferrin, Tris (2,2-bipyridyl) dichlororuthenium(II) hexahydrate (Rubpy), Triton X-100, 1-ethyl-3-[3-dimethylaminopropyl] carbodiimide hydrochloride (EDC), and *N*-hydroxysuccinimide (NHS) were obtained from Sigma-Aldrich. Transwell with 0.4 μm pore polycarbonate membrane was obtained from Millipore. The bEnd.3 cell line (BALB/c cerebral endothelial cells) was purchased from ATCC. Male Balb/c mice (7−8 weeks, 20 g) were purchased from Shanghai Silaike Experimental Animals Co., Ltd. Other chemicals, if not specified, were all commercially available. All reagents were analytical grade and used without any purification.

Preparation of PSiNPs with Different Diameters. First, SiNPs of three different sizes with free carboxyl groups were synthesized by changing the water-to-surfactant molar ratio using the water-in-oil (W/O) microemulsion method. Briefly, a solution containing 7.5 mL of cyclohexane, 1.8 mL of Triton X-100 and 1.6 mL of *n*-hexanol was mixed with 160, 400, and 1120 μL of water (with the water-to-surfactant molar ratio 5, 10, 25, respectively) and stirred for 5 min, followed by the addition of 80 μL of 0.1 M Rubpy dye solution. After stirring for 30 min, 200 μL of tetraethyl orthosilicate (TEOS) and 100 μL of concentrated NH_4OH to initiate polymerization. The reaction was allowed to continue for 24 h, and 50 μL of TEOS and 100 μL of *N*-[(3-trimethoxysilyl)propyl] ethylenediamine triacetic acid were then added to form SiNPs with free carboxyl groups via hydrolysis. The concentration of SiNPs was measured by dispersion method and calculated according to the following formula (eq 1). W_1, W_2, and V represented the mass of the empty tube, the mass of the tube containing SiNPs added after drying overnight under vacuum, and the volume of SiNPs added, respectively.

$$\text{concentration of SiNPs(mg/mL)} = (W_2 - W_1)/V \quad (1)$$

PSiNPs were prepared by the classical (EDC/sulfo-NHS)-mediated amidation conjugation reaction. Briefly, 450 μL EDC (50 μg/μL) and 450 μL NHS (50 μg/μL) were added to 600 μL MES buffer (pH 6.0) containing 6 mg of SiNPs of one certain size. After approximately 30 min, the activated SiNPs were washed and resuspended in 1200 μL of MES solution. Then, 600 μL of 50 μg/μL PEG solution was added to 400 μL of 5 mg/mL activated SiNPs and incubated with gentle shaking overnight at 4 °C. After repetitive washing and removal of unreacted PEG by centrifugation, the PSiNPs were redissolved in PBS for future usage. The concentration of PSiNPs was roughly equal to that of SiNPs.

Construction and Characterization of BBB Models. For construction of the BBB models, transwell inserts were first placed into a culture plate well, and DMEM growth medium was added to the basolateral side of each well until the membrane in each insert was completely moistened with the growth medium. Then bEnd.3 cells were seeded onto the inside of the insert above the membrane at an initial density of 1×10^5 cells/well and cultured in DMEM growth medium with 10% fetal bovine serum. Cultures were maintained at 37 °C and 5% CO_2 in a humidified incubator. The growth medium was changed every day, and the cells were grown to a compact monolayer for about 12 days.

For characterization of the BBB models, the cell morphology of BBB models was initially observed by phase contrast optical microscopy (PCOM). To further determine the BBB tight junction, transmission electron microscopy (TEM) analyses were performed. Briefly, the cell monolayer with transwell membrane was clipped and washed with PBS, then fixed in 2.5% glutaraldehyde for 2 h and postfixed with 2% osmium tetroxide for 1 h. Afterward, the membrane was dehydrated through a graded series of acetone (70%, 80%, 90%, 100%, 100%), embedded in araldite resin, and sectioned with an ultramicrotome. The prepared ultrathin sections (70 nm) were imaged by transmission electron microscopy (JEM-2100) at an accelerating voltage of 80 kV. For determining the integrity of BBB models, transendothelial electrical resistance (TEER) experiments were performed. A device with two electrodes was used, one placed in the apical side with the other in the basolateral side chamber. TEER values were automatically obtained by this device.

Integrity of the BBB Incubation with Three Different Sizes of PSiNPs. TEER experiments were performed to evaluate the effects of PSiNPs on the integrity of the BBB. Briefly, PSiNPs of three different sizes in DMEM without fetal bovine serum were added to the apical side chamber of the BBB models, with final concentrations of 0.2 mg/mL. DMEM medium without fetal bovine serum was used as the blank control. Then, the PSiNPs with three different sizes were incubated with the BBB models at 37 °C for 12 h with TEER values measured once an hour.

BBB Model Studies with PSiNPs in Vitro. PSiNPs with sizes of 100, 50, and 25 nm in DMEM without fetal bovine serum were added to the apical side chamber of the BBB models, with final concentrations of 0.2 mg/mL respectively. DMEM medium without fetal bovine serum was used as the blank control. After approximately

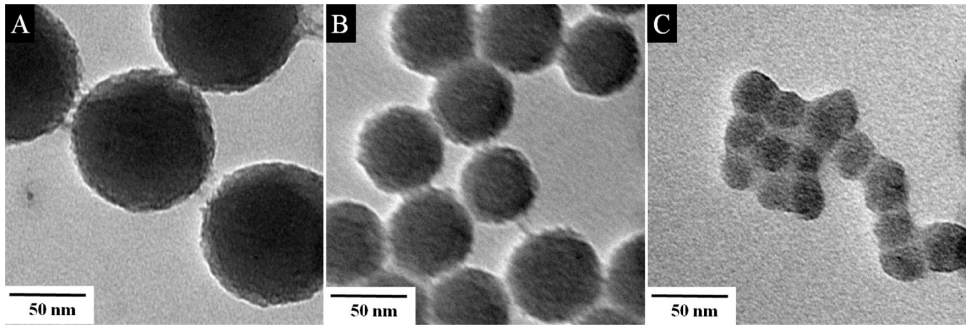

Figure 1. Transmission electron microscopy images of PSiNPs (A, 100; B, 50; C, 25 nm).

12 h of incubation, the medium containing PSiNPs in the basolateral side was collected and detected by fluorescence spectrometry, using Rubpy dye doped in the PSiNPs as a fluorescent signal indicator. The medium containing PSiNPs with final concentrations of 0.2 mg/mL and the control medium were also detected by fluorescence spectrometry. On the basis of the linear dependence of the fluorescence intensity of PSiNPs on the concentration in medium over the effective concentration range, the transport efficiency of PSiNPs across the BBB was calculated according to the following formula (eq 2), where F_{bs}, F_{tt} and F_{ct} represent the fluorescence intensity of the basolateral medium containing PSiNPs, the medium containing 0.2 mg/mL PSiNPs, and the control medium, respectively.

$$\text{transport efficiency}\ (\%) = (F_{bs} - F_{ct})/(F_{tt} - F_{ct}) \times 100\% \qquad (2)$$

Determination of Cellular Uptake of PSiNPs by bEnd.3 Cells. To determine the uptake of PSiNPs by bEnd.3 cells, the bEnd.3 cells were incubated with 0.2 mg/mL of suspensions containing three different sizes of PSiNPs in DMEM without fetal bovine serum at 37 °C for 4 h. Treated cells were then washed three times with cold PBS to remove excess PSiNPs. The Rubpy fluorescent dye incorporated in PSiNPs served as a marker to determine their cellular uptake and analyzed by laser scanning confocal microscopy.

Animal Experiments in Vivo. Animal experiments were performed to further investigate the transport of PSiNPs across the BBB. The athymic BALB/c mice with an average weight of 20 g were selected as animal models. In detail, mice were first anesthetized intraperitoneally with 2% pentobarbital and 0.08% promethazine hydrochloride. Then, PSiNPs (three different sizes) in PBS buffer were injected into the mice via carotid artery at 0.03 mg/g (NP weight/animal weight), respectively. Whole body images were acquired 15 min, 1 h, and 3 h postinjection and analyzed using the Maestro in vivo imaging system (CRI, Inc., excitation, 465−495 nm, emission, 550−700 nm). After in vivo imaging, mice were sacrificed by dislocation. The dissected organs of the brain were imaged with the Maestro imaging system as described above. The mean fluorescence intensity was analyzed using Maestro 2.10 image analysis software.

RESULTS AND DISCUSSION

Characterization of PSiNPs. PSiNPs with three different sizes were characterized by transmission electron microscopy (TEM, JEM-1400). The morphological analysis showed that all of them were well-dispersed spherical nanoparticles and uniform in size. The average diameters were 97 ± 2, 54 ± 3, and 27 ± 2 nm, respectively (Figure 1A−C). For convenience, diameters of three different size PSiNPs were marked as 100, 50, and 25 nm in the following text, respectively. The zeta potential of SiNPs before and after PEG bioconjugation was determined using Malvern Zetasizer (Zetasizer NanoZS90). According to the values of the zeta potential (Table 1), the surface charges of SiNPs with three different sizes decreased after bioconjugation, indicating the successful modification by PEG.

Table 1. Surface Charge of the SiNPs and PSiNPs

	zeta potential (mV)	
diameters	SiNPs	PSiNPs
100 nm	−39.7 ± 0.8	−31.9 ± 1
50 nm	−37.4 ± 1.2	−21.6 ± 2.4
25 nm	−34.5 ± 3.1	−19.4 ± 1.8

Characterization of the BBB Model. The BALB/c brain endothelial cells (bEnd.3 cell line) have commonly been used for in vitro BBB models with transwell membranes. Moreover, the bEnd.3 monolayer is especially suitable for studying solute and particle transport across the BBB.[37−40] Our in vitro BBB model was based on the culture of the well-established bEnd.3 cell line with transwell inserts. As shown in Figure 2A, brain endothelial cells showed a spindle shaped morphology followed by 12 days of culture. The inter-endothelial cleft (width of less

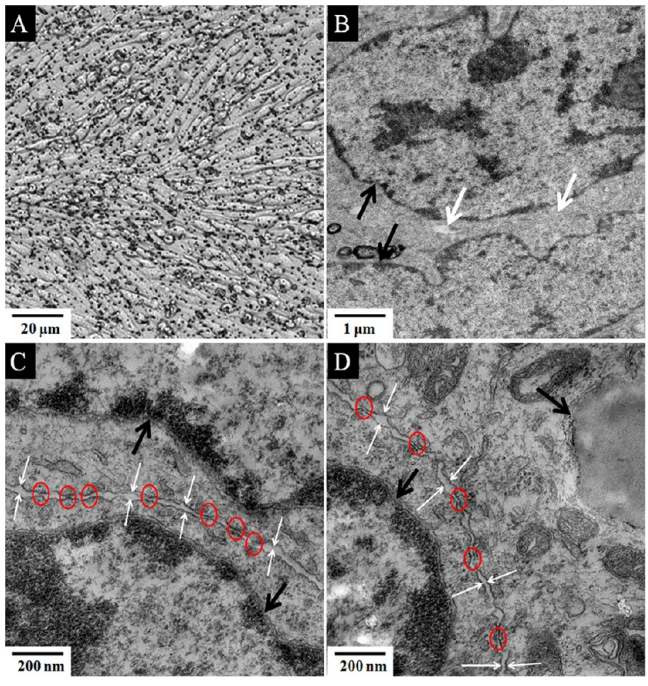

Figure 2. Microscopy of brain endothelial cells grown upon transwell membranes to monolayer confluency on 12th day (A). TEM images of tight junction (circled in red) of BBB models at high magnification (B) 6000×, (C)10 000×, (D)10 000×. Width of inter-endothelial cleft was less than 18 nm (between the two white arrows).Opening width of tight junction was less than 8 nm (circled in red). Black arrow marks represent cell nucleolus.

dx.doi.org/10.1021/am405219u | ACS Appl. Mater. Interfaces 2014, 6, 2131−2136

than 18 nm) with a tight junction (opening width of less than 8 nm) between two adjacent endothelial cells, which formed a belt-like structure, could also be easily observed by TEM (Figure 2B–D). The above values were consistent with the anatomical parameters of bEnd.3 monolayer as reported in the literature.[37] The results showed that the model is suitable for basic research of testing the interaction between the BBB and the NPs. Commonly, the TEER can be used to evaluate the integrity of the in vitro BBB model, which is expressed as measured resistance multiplied by the area of the endothelial monolayer with units of $\Omega \times cm^2$.[41−43] Previous studies indicated that the confluence of brain endothelial cells plated on transwell membranes and cultured for 8−12 days could be confirmed by a TEER value of over 200 $\Omega \times cm^2$.[44] In our model, a higher TEER value of above 300 $\Omega \times cm^2$ was detected on day 12, illustrating that the confluent monolayer could adequately serve as an in vitro model for investigating the transport of NPs. Therefore, the BBB model with TEER value above 300 $\Omega \times cm^2$ was selected for subsequent experiments.

Biocompatibility of PSiNPs with BBB. The biocompatibility mainly refers to the integrity of the BBB during the incubation with PSiNPs. Galla et al. reported that the presence of surface-modified Fe_3O_4 nanoparticles had no effect on the integrity of an in vitro BBB model. On the basis of the barrier integrity, the study investigated the permeation of particles across BBB.[45] Systematic studies have been carried out on the bioeffects of the SiNPs with cells. Results indicated that the biocompatibility of SiNPs is concentration dependent, with no measurable cytotoxic effects of SiNPs being observed on the growth and proliferation of cells over a certain range of concentrations.[46,47] Here, PSiNPs with concentrations of 0.2 mg/mL were selected to be incubated with the BBB model and to further confirm PSiNPs at this concentration had no effect on BBB integrity. TEER measurements were performed for three different sizes of PSiNPs with final concentrations of 0.2 mg/mL incubated with the BBB model, and DMEM medium without fetal bovine serum was provided as the blank control. All the TEER data were further normalized to a range between 0 and 1 for better analysis. As shown in Figure 3, the TEER values of all nanoparticle groups showed similar trends in comparison with the control group during the 12 h incubation period. The results indicated that the incubation of PSiNPs with final concentrations of 0.2 mg/mL did not affect the integrity of the BBB model. PSiNPs with three different sizes of 100, 50, and 25 nm have good biocompatibility with BBB.

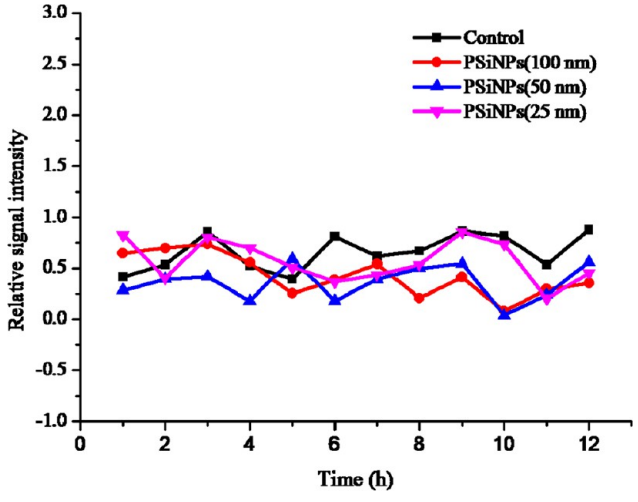

Figure 3. Normalized TEER values of BBB models during incubation with 0.2 mg/mL PSiNPs for biocompatibility evaluation. DMEM medium served as control.

Transport of PSiNPs with Different Sizes across the BBB in Vitro. To determine if the PSiNPs could pass through the BBB and the influence of particle size, transport studies of 100, 50, and 25 nm PSiNPs across the BBB were performed using the in vitro BBB model after 12 h incubation. The permeating efficiency calculated using eq 1 for PSiNPs with three different sizes through the BBB model is shown in Table 2 and Figure 4. The results showed that PSiNPs could pass through the BBB model and the transport efficiency of PSiNPs was size dependent. Maximum efficiency was observed for 25 nm PSiNPs. Increase in particle size of PSiNPs resulted in decrease in the permeation efficiency through the BBB. The 100 nm PSiNPs had lowest transport efficiency of 10.6%. The 50 nm PSiNPs showed intermediate transport efficiency of 19.2%, whereas the transport efficiency of 25 nm PSiNPs was 26.1%, 2.5 fold higher than that of 100 nm PSiNPs.

Table 2. Transport Efficiency of PSiNPs across the BBB in Vitro

200 μg/mL PSiNPs (initial) in the apical medium	PSiNPs concentration of the basolateral medium (μg/mL)	transport efficiency (%)
PSiNP(100 nm)	21.2 ± 4.2	10.6 ± 2.1
PSiNP(50 nm)	38.4 ± 18.4	19.2 ± 9.2
PSiNP(25 nm)	52.2 ± 17.9	26.1 ± 8.9

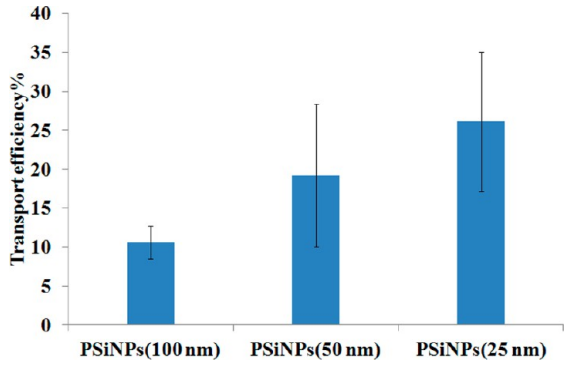

Figure 4. Transport efficiency of PSiNPs across the BBB in vitro.

Cellular Uptake of Nanoparticles by bEnd.3 Cells. Crossing the BBB is based on the interactions between NPs and the BBB and on their pathways of transcytosis.[22] Transcytosis in endothelial cells starts with internalization of extracellular cargo into the cells by vesicular carriers. The cargo is subsequently processed via different pathways to appropriate intracellular organelles and recycled, degraded, or transcytosed to the contralateral side.[48] To determine whether the PSiNPs were internalized into brain capillary endothelial cells, the cellular uptake of the 100, 50, and 25 nm PSiNPs by brain capillary endothelial cells was evaluated for 4 h of incubation, because 4 h of incubation was considered as the optimum period of cellular uptake of PSiNPs by cells.[49] As shown in Figure 5, all three sizes of PSiNPs could be taken up by bEnd.3 cells. The images of the red fluorescence from 25 nm PSiNPs revealed a relatively effective uptake by brain capillary endothelial cells, as compared with 50 and 100 nm PSiNPs. The results indicated that cellular uptake of small nanoparticles

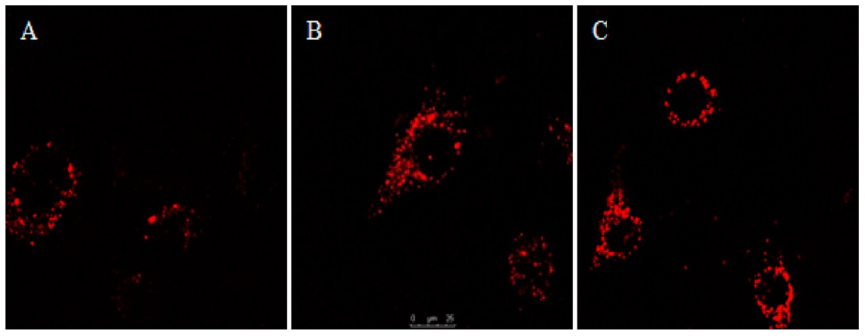

Figure 5. Confocal fluorescence images of bEnd.3 cells after treatment with 0.2 mg/mL PSiNPs for 12 h. (A) 100 nm PSiNPs, (B) 50 nm PSiNPs, (C) 25 nm PSiNPs.

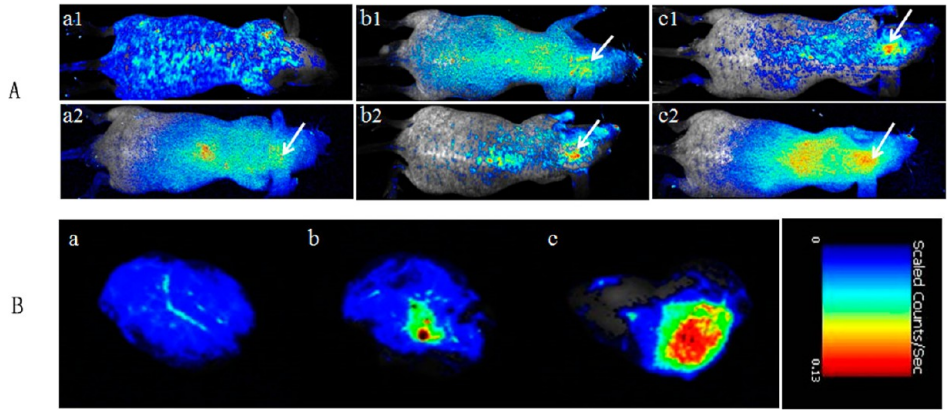

Figure 6. (A) In vivo back imaging of brain deposit of PSiNPs at different time points (1 representing 15 min; 2 representing 1 h) after injection via carotid artery. (a) 100 nm, (b) 50 nm, (c) 25 nm. Arrows mark the location of the brain. B. Ex vivo optical imaging of resected brain. (a), (b), (c) representing PSiNPs of 100, 50, and 25 nm, respectively.

by brain capillary endothelial cells was more favorable than that of large NPs, indicating size-dependent transport efficiency.

Transport of PSiNPs across BBB in Vivo. To confirm the transport of PSiNPs with three different sizes across the BBB, animal studies were further carried out by noninvasive in vivo and ex vivo imaging. The results of in vivo back imaging are shown in Figure 6A, as indicated by the fluorescence signal of Rubpy entrapped in PSiNPs. The brain deposit of PSiNPs in mice shown in Figure 6 changed significantly with respect to time during a 1 h imaging period. For 100 nm PSiNPs, after 15 min from injection via carotid artery, there was no significant fluorescence signal of PSiNPs in the brain region. After 1 h, the fluorescence emitting from the brain gradually increased, indicating that the PSiNPs have been deposited in the brain. In the case of 50 nm PSiNPs, fluorescence from PSiNPs was observed in the brain after 15 min injection. Then the fluorescence signal of PSiNPs in the brain was greatly increased after 1 h. Obvious distribution of 25 nm PSiNPs was found in the brain after both 15 min and 1 h injection. Compared with 100 and 50 nm PSiNPs, 25 nm PSiNPs exhibited significant distribution in the brain within 1 h postinjection, indicating that 25 nm PSiNPs have higher transport efficiency across the BBB than PSiNPs of 100 or 50 nm. The result was in good agreement with the brain tissue distribution of differently sized gold nanoparticles (15, 50, 100, and 200 nm) after intravenous injection in mice.[50]

Further examination of ex vivo brain images was performed to provide additional evidence for the transport efficiency of different sized PSiNPs across the BBB. As shown in Figure 6B, the fluorescence intensity of 25 nm PSiNPs in the brain was maximum, whereas intermediate for 50 nm PSiNPs and minimal for 100 nm PSiNPs. These results indicate that the transport efficiency of PSiNPs across the BBB is inversely dependent on the particle size, consistent with results of the in vitro experiments.

CONCLUSIONS

In summary, the transport of PSiNPs with diameters of 100, 50, and 25 nm across the BBB was evaluated both in vitro and in vivo. The results indicate that PSiNPs can traverse the BBB in vitro and in vivo, and that the transport efficiency is size dependent. An increase in particle size of PSiNPs decreases the transport efficiency across the BBB. Moreover, consistent with the ability of PSiNPs to cross the BBB, the 25 nm nanoparticles showed higher efficiency in uptake by brain capillary endothelial cells than 100 and 50 nm particles. This work points to the potential application of small sized silica nanoparticles in delivery of diagnostic and therapeutic agents across the BBB. Even though these results for biocompatible silica nanoparticles indicate their utility in brain imaging or drug delivery, it is important to consider neurotoxicity issues. Therefore, we will investigate the neurotoxicity of small sized silica nanoparticles at the cell and small animal levels in the future.

AUTHOR INFORMATION

Corresponding Authors

*T. Ji. E-mail: skysea_ji@sina.com.
*C. Yang. E-mail: cyyang@xmu.edu.cn.

Author Contributions

†These authors contributed equally to this work.

Notes

The authors declare no competing financial interest.

■ ACKNOWLEDGMENTS

We thank the National Basic Research Program of China (81101904, 21205100, 21275122), 973 Program of China (2010CB732402, 2013CB933703), National Instrumentation Program (2011YQ03012412), and National Science Foundation for Distinguished Young Scholars of China (21325522).

■ REFERENCES

(1) Ballabh, P.; Braun, A.; Nedergaard, M. *Neurobiol. Dis.* **2004**, *16*, 1−13.
(2) Petty, M. A.; Lo, E. H. *Prog. Neurobiol.* **2002**, *68*, 311−323.
(3) Yoshikawa, T.; Sakaeda, T.; Sugawara, T.; Hirano, K.; Stella, V. J. *Adv. Drug Delivery Rev.* **1999**, *36*, 255−275.
(4) Sanovich, E.; Bartus, R. T.; Friden, P. M.; Dean, R. L.; Le, H. Q.; Brightman, M. W. *Brain Res.* **1995**, *705*, 125−135.
(5) Tang, S. C.; Lankheet, N. A.; Poller, B.; Wagenaar, E.; Beijnen, J. H.; Schinkel, A. H. *J. Pharmacol. Exp. Ther.* **2012**, *341*, 164−173.
(6) Holmes, D. *Lancet Neurol.* **2013**, *12*, 31−32.
(7) Re, F.; Gregori, M.; Masserini, M. *Nanomedicine* **2012**, *8* (Suppl 1), S51−58.
(8) Navalakhe, R. M.; Nandedkar, T. D. *Indian J. Exp. Biol.* **2007**, *45*, 160.
(9) Montet, X.; Funovics, M.; Montet-Abou, K.; Weissleder, R.; Josephson, L. *J. Med. Chem.* **2006**, *49*, 6087−6093.
(10) Swierczewska, M.; Choi, K. Y.; Mertz, E. L.; Huang, X.; Zhang, F.; Zhu, L.; Yoon, H. Y.; Park, J. H.; Bhirde, A.; Lee, S.; Chen, X. *Nano Lett.* **2012**, *12*, 3613−3620.
(11) Yang, Y.; Velmurugan, B.; Liu, X.; Xing, B. *Small* **2013**, *9*, 2937−2944.
(12) Santra, S.; Yang, H.; Stanley, J. T.; Holloway, P. H.; Moudgil, B. M.; Walter, G.; Mericle, R. A. *Chem. Commun.* **2005**, 3144−3146.
(13) Schroeder, U.; Sommerfeld, P.; Ulrich, S.; Sabel, B. A. *J. Pharm. Sci.* **1998**, *87*, 1305−1307.
(14) Broadwell, R. *Acta Neuropathol.* **1989**, *79*, 117−128.
(15) Jones, A. R.; Shusta, E. V. *Pharm. Res.* **2007**, *24*, 1759−1771.
(16) Georgieva, J. V.; Kalicharan, D.; Couraud, P. O.; Romero, I. A.; Weksler, B.; Hoekstra, D.; Zuhorn, I. S. *Mol. Ther.* **2011**, *19*, 318−325.
(17) Sadekar, S.; Ghandehari, H. *Adv. Drug Delivery Rev.* **2012**, *64*, 571−588.
(18) Kotzé, A. F.; Lueßen, H. L.; de Leeuw, B. J.; de Boer, B. G.; Coos Verhoef, J.; Junginger, H. E. *J. Controlled Release* **1998**, *51*, 35−46.
(19) Treat, L. H.; McDannold, N.; Zhang, Y.; Vykhodtseva, N.; Hynynen, K. *Ultrasound Med. Biol.* **2012**, *38*, 1716−1725.
(20) Adamson, R. H.; Lenz, J. F.; Zhang, X.; Adamson, G. N.; Weinbaum, S.; Curry, F. E. *J. Physiol.* **2004**, *557*, 889−907.
(21) Kreuter, J. *Adv. Drug Delivery Rev.* **2001**, *47*, 65−81.
(22) Masserini, M. *ISRN Biochem.* **2013**, *2013*, 1−18.
(23) Blasi, P.; Giovagnoli, S.; Schoubben, A.; Ricci, M.; Rossi, C. *Adv. Drug Delivery Rev.* **2007**, *59*, 454−477.
(24) Hasadsri, L.; Kreuter, J.; Hattori, H.; Iwasaki, T.; George, J. M. *J. Biol. Chem.* **2008**, *284*, 6972−6981.
(25) Liu, D.; He, X.; Wang, K.; He, C.; Shi, H.; Jian, L. *Bioconjugate Chem.* **2010**, *21*, 1673−1684.
(26) Peng, J.; He, X.; Wang, K.; Tan, W.; Wang, Y.; Liu, Y. *Anal. Bioanal. Chem.* **2007**, *388*, 645−654.
(27) Zhao, X.; Tapec-Dytioco, R.; Tan, W.; Ultrasensitive, DNA *J. Am. Chem. Soc.* **2003**, *125*, 11474−11475.
(28) Santra, S.; Zhang, P.; Wang, K.; Tapec, R.; Tan, W. *Anal. Chem.* **2001**, *73*, 4988−4993.
(29) He, X.; Nie, H.; Wang, K.; Tan, W.; Wu, X.; Zhang, P. *Anal. Chem.* **2008**, *80*, 9597−9603.
(30) Wang, K.; He, X.; Yang, X.; Shi, H. *Acc. Chem. Res.* **2013**, *46*, 1367−1376.
(31) Peng, F.; Su, Y.; Wei, X.; Lu, Y.; Zhou, Y.; Zhong, Y.; Lee, S. T.; He, Y. *Angew. Chem., Int. Ed.* **2013**, *52*, 1457−1461.
(32) Su, S.; Wei, X.; Zhong, Y.; Guo, Y.; Su, Y.; Huang, Q.; Lee, S. T.; Fan, C.; He, Y. *ACS Nano* **2012**, *6*, 2582−2590.
(33) Tenzer, S.; Docter, D.; Rosfa, S.; Wlodarski, A.; Kuharev, J.; Rekik, A.; Knauer, S. K.; Bantz, C.; Nawroth, T.; Bier, C.; Sirirattanapan, J.; Mann, W.; Treuel, L.; Zellner, R.; Maskos, M.; Schild, H.; Stauber, R. H. *ACS Nano* **2011**, *5*, 7155−7167.
(34) Desai, M. P.; Labhasetwar, V.; Amidon, G. L.; Levy, R. J. *Pharm. Res.* **1996**, *13*, 1838−1845.
(35) Panyam, J.; Dali, M. M.; Sahoo, S. K.; Ma, W.; Chakravarthi, S. S.; Amidon, G. L.; Levy, R. J.; Labhasetwar, V. *J. Controlled Release* **2003**, *92*, 173−187.
(36) Brigger, I.; Morizet, J.; Aubert, G.; Chacun, H.; Terrier-Lacombe, M. J.; Couvreur, P.; Vassal, G. *J. Pharmacol. Exp. Ther.* **2002**, *303*, 928−936.
(37) Yuan, W.; Li, G.; Gil, E. S.; Lowe, T. L.; Fu, B. M. *Ann. Biomed. Eng.* **2010**, *38*, 1463−1472.
(38) Brown, R. C.; Morris, A. P.; O'Neil, R. G. *Brain Res.* **2007**, *1130*, 17−30.
(39) Li, G.; Simon, M. J.; Cancel, L. M.; Shi, Z. D.; Ji, X.; Tarbell, J. M.; Morrison, B., 3rd; Fu, B. M. *Ann. Biomed. Eng.* **2010**, *38*, 2499−2511.
(40) Soga, N.; Connolly, J. O.; Chellaiah, M.; Kawamura, J.; Hruska, K. A. *Cell Commun. Adhes.* **2001**, *8*, 1−13.
(41) Franke, H.; Galla, H.-J.; Beuckmann, C. T. *Brain Res. Protoc.* **2000**, *5*, 248−256.
(42) Qiao, R.; Jia, Q.; Hüwel, S.; Xia, R.; Liu, T.; Gao, F.; Galla, H.-J.; Gao, M. *ACS Nano* **2012**, *6*, 3304−3310.
(43) Fillebeen, C.; Descamps, L.; Dehouck, M.-P.; Fenart, L.; Benaïssa, M.; Spik, G.; Cecchelli, R.; Pierce, A. *J. Biol. Chem.* **1999**, *274*, 7011−7017.
(44) Wong, A. D.; Ye, M.; Levy, A. F.; Rothstein, J. D.; Bergles, D. E.; Searson, P. C. *Front. Neuroeng.* **2013**, *6*, 7.
(45) Qiao, R.; Jia, Q.; Huwel, S.; Xia, R.; Liu, T.; Gao, F.; Galla, H. J.; Gao, M. *ACS Nano* **2012**, *6*, 3304−3310.
(46) He, X.; Liu, F.; Wang, K.; Ge, J.; Qin, D.; Gong, P.; Tan, W. *Chin. Sci. Bull.* **2006**, *51*, 1939−1946.
(47) Barandeh, F.; Nguyen, P.-L.; Kumar, R.; Iacobucci, G. J.; Kuznicki, M. L.; Kosterman, A.; Bergey, E. J.; Prasad, P. N.; Gunawardena, S. *PloS one* **2012**, *7*, e29424.
(48) Muro, S.; Koval, M.; Muzykantov, V. *Curr. Vasc. Pharmacol.* **2004**, *2*, 281−299.
(49) Tian, X.-h.; Wei, F.; Wang, T.-x.; Wang, P.; Lin, X.-n.; Wang, J.; Wang, D.; Ren, L. *Int. J. Nanomed.* **2012**, *7*, 1031.
(50) Sonavane, G.; Tomoda, K.; Makino, K. *Colloids Surf., B* **2008**, *66*, 274−280.